

# The resistance of an aluminide coating on a high-strength ASTM A29 steel subjected to a temperature of 850

*by* Sugiyanto Sugiyanto

---

**Submission date:** 06-Aug-2019 09:56AM (UTC+0800)

**Submission ID:** 1157957592

**File name:** 3.\_Mater\_Res\_Express.pdf (1,020.16K)

**Word count:** 3847

**Character count:** 23655

ACCEPTED MANUSCRIPT • OPEN ACCESS

5

## The resistance of an aluminide coating on a high-strength ASTM A29 steel subjected to a temperature of 850<sup>o</sup>C

1

To cite this article before publication: Mohammad Badaruddin *et al* 2019 *Mater. Res. Express* in press <https://doi.org/10.1088/2053-1591/ab2508>

### Manuscript version: Accepted Manuscript

Accepted Manuscript is "the version of the article accepted for publication including all changes made as a result of the peer review process, and which may also include the addition to the article by IOP Publishing of a header, an article ID, a cover sheet and/or an 'Accepted Manuscript' watermark, but excluding any other editing, typesetting or other changes made by IOP Publishing and/or its licensors"

This Accepted Manuscript is © 2019 IOP Publishing Ltd.

As the Version of Record of this article is going to be / has been published on a gold open access basis under a CC BY 3.0 licence, this Accepted Manuscript is available for reuse under a CC BY 3.0 licence immediately.

Everyone is permitted to use all or part of the original content in this article, provided that they adhere to all the terms of the licence <https://creativecommons.org/licenses/by/3.0>

Although reasonable endeavours have been taken to obtain all necessary permissions from third parties to include their copyrighted content within this article, their full citation and copyright line may not be present in this Accepted Manuscript version. Before using any content from this article, please refer to the Version of Record on IOPscience once published for full citation and copyright details, as permissions may be required. All third party content is fully copyright protected and is not published on a gold open access basis under a CC BY licence, unless that is specifically stated in the figure caption in the Version of Record.

View the [article online](#) for updates and enhancements.

The resistance of an aluminide coating on a high-strength ASTM A29 steel subjected to a temperature of 850°C

Mohammad Badaruddin <sup>a,\*</sup>, Sugiyanto <sup>a</sup>, Dwi Asmi <sup>b</sup>

<sup>a</sup>Department of Mechanical Engineering, Faculty of Engineering, Universitas Lampung, Bandar Lampung 35145, Indonesia

<sup>b</sup>Department of Physics, Faculty of Mathematics and Science, Universitas Lampung, Bandar Lampung 35145, Indonesia

\*Corresponding author: Jalan Prof. S. Brojonegoro No. 1, Bandar Lampung 35145, Indonesia  
Telp.: +62-721-704947, Fax.: +62-721-704947  
E-mail address: [mbruddin@eng.unila.ac.id](mailto:mbruddin@eng.unila.ac.id) (M. Badaruddin).

### Abstract

An ASTM A29 steel was coated with aluminide by dipping in a molten Al bath at 700°C for 16 s. The resistance of ASTM A29 steel to high-temperature oxidation drastically decreased upon oxidation at 850°C for 12 h, whereas the oxidation resistance of the aluminised steel subjected to hot dipping was higher (by 25-fold). The external part of the aluminide layer, which consists of Fe<sub>2</sub>Al<sub>5</sub>, FeAl<sub>2</sub>, and FeAl(Cr,Si) phases scattered in the Fe<sub>2</sub>Al<sub>5</sub> phase, was formed through the outward diffusion of Al and inward diffusion of Fe. The Fe<sub>2</sub>Al<sub>5</sub> phase played an important role as a reservoir of Al atoms that form the alumina (Al<sub>2</sub>O<sub>3</sub>) scale, while Cr and Fe from the FeAl(Cr,Si) particles and accelerated the conversion of the metastable  $\theta$ -Al<sub>2</sub>O<sub>3</sub> phase to a stable  $\alpha$ -Al<sub>2</sub>O<sub>3</sub> phase. Consequently, the parabolic rate constants of aluminised steel decreased with extended oxidation time.

*Keywords: ASTM A29 steel, aluminide layer, high-temperature, oxidation resistance, alumina*

## 1. Introduction

1  
2  
3 A high strength ASTM A29 low alloy steel with a 1.10 Cr-0.25 Mo (wt.%) can be a candidate  
4 material as replacement of high Cr-Mo steel grades and stainless-steel grades for high-temperature  
5 material applications in the petrochemical industry, power plants and transportations sectors. The  
6 ASTM A29 steel has good mechanical properties and is cheaper than those of high Cr-Mo steel  
7 grades and stainless-steel grades. However, the low Cr concentration in this steel is a critical issue,  
8 which limits its industrial application. Mazrouee and Raman [1] reported that the oxidation  
9 resistance of a 1.25Cr-0.5Mo steel exhibited a significant decrease in the temperature range of  
10 500–600°C. At higher temperatures, the rapid oxidation kinetics for the chrome-moly steels with  
11 0.5-9% Cr and 0.5-1% Mo were attributed to the loss of the protective Cr<sub>2</sub>O<sub>3</sub> layer, which led to  
12 growing non-protective (Fe<sub>2</sub>O<sub>3</sub>), Fe<sub>3</sub>O<sub>4</sub>, and (Fe,Cr)<sub>3</sub>O<sub>4</sub> scales. Therefore, the application of these  
13 steels is restricted above 600°C [1–4].

14  
15  
16  
17  
18  
19  
20  
21  
22  
23  
24  
25  
26  
27  
28 To widen industrial applications in the temperature range of 700–850°C, the oxidation  
29 resistance of ASTM A29 steel needs to be improved by hot-dip aluminising (HDA) coating. HDA  
30 coating has been reported to be a simple, cost-effective method for improving the high-temperature  
31 resistance of steel and its alloys by forming a protective Al<sub>2</sub>O<sub>3</sub> scale on the outer layer [5–7]. There  
32 are two types of HDA steel coating: (1) the aluminised Type 1 steel uses Al-(3-10%)Si, and (2)  
33 the aluminised Type 2 steel uses relatively high purity Al. Adding a certain amount of Si into a  
34 molten Al bath reduces the thickness of the aluminide coating on the steel substrate [8,9], which  
35 thins the aluminide coating, a pre-requisite to further manufacturing of aluminised steel  
36 components [10]. Therefore, an HDA coating with Al-Si is normally applied to low carbon steel,  
37 which is mainly used for automotive exhaust systems, furnace heat exchangers and other heat-  
38 resistant applications at 700°C [5,6]. However, the high-Si content in the intermetallic of FeAl  
39 layer growing on the low carbon steel substrate [5,6] and on the high Cr-Mo steel substrate [7,11]  
40  
41  
42  
43  
44  
45  
46  
47  
48  
49  
50  
51  
52  
53  
54  
55  
56  
57  
58  
59  
60

1  
2  
3 during oxidation in temperature range of 750–850°C had a detrimental effect, which led to the  
4 breakdown of protective  $\text{Al}_2\text{O}_3$  layer due to local formation of iron oxide nodules. Therefore, the  
5 aluminised Type 2 steel has better oxidation resistance than that of the aluminised Type 1 steel  
6 [12]. Additionally, the aluminising Type 2 coating was applied to high strength AISI 4130 steel,  
7 which combines the strength of steel substrate and aluminide coating protections for superior hot-  
8 corrosion resistance [13]. Because the thickness of the aluminide layer on the steel substrate  
9 determines the steel's mechanical properties [10], all industrial hot-dip aluminising type 2  
10 processes allow the strict control of the coating reaction, by shortening the dipping time in few  
11 seconds.  
12  
13  
14  
15  
16  
17  
18  
19  
20  
21  
22

23  
24 Only a few publications <sup>9</sup> on the high-temperature oxidation of aluminising Type 2 coating on  
25 high strength steel grades with the low Cr-Mo contents are available in the literature. Therefore,  
26 we experimentally investigated the resistance of aluminised Type 2 ASTM A29 steel on high-  
27 temperature oxidation in ambient air at 850°C. A thermogravimetric analyser (TGA) was adopted  
28 to evaluate the oxidation kinetics of an ASTM A29 steel with and without aluminising coating.  
29 The microstructures, chemical composition and surface morphology of the aluminide layers after  
30 oxidation were examined.  
31  
32  
33  
34  
35  
36  
37  
38  
39  
40  
41  
42

## 43 2. Experimental procedure

44  
45 A commercial ASTM A29 steel with chemical compositions of 0.3C-1.10Cr-0.25Mo-0.60Mn-  
46 0.035P-0.04S-0.30Si (wt.%) was cut into specimens with 20 mm × 10 mm × 2 mm dimensions. A  
47 hole (1 mm diameter) was drilled into each specimen. The specimen surface was polished using  
48 500–1000 emery paper and later ultrasonically cleaned using acetone and ethanol for a few  
49 seconds. Before coating, all specimens were ultrasonically neutralised using a 5% NaOH and a  
50  
51  
52  
53  
54  
55  
56  
57  
58  
59  
60

1  
2  
3 10% H<sub>3</sub>PO<sub>4</sub> solution for a few seconds. Next, the specimen surface was covered with an aluminium  
4 welding flux. The specimen was hung on a mini crane (Linear head (2FL10N-5 model) driven by  
5 a motor (2RK6RGN-CW2L model, with MSC controller) using a stainless-steel wire with 1 mm  
6 diameter. A motor automatically drove the mini crane at a constant speed of 14.3 mm/min, dipping  
7 the specimen into a molten Al-0.5Si (wt.%) bath at 700°C for 16 s. After the specimen was dipped,  
8 it was automatically pulled out from a molten Al bath and then cooled to room temperature. The  
9 oxide remaining on the specimen surface <sup>3</sup> was then cleaned using a phosphoric acid/nitric  
10 acid/water solution (1:1:1 v/v) at room temperature.  
11  
12  
13  
14  
15  
16  
17  
18  
19  
20

21 To investigate the oxidation kinetics of the steels with and without the aluminium coating,  
22 specimens were subjected to air <sup>6</sup> oxidation at 850°C for 12 h using a TGA (Pyris 6 model). <sup>18</sup> To  
23 evaluate the phase transformation and microstructures of the aluminide layer, aluminised steel  
24 specimens were oxidised <sup>6</sup> in a box furnace at 850°C for various times (1, 5 and 12 h) under static  
25 air. After the aluminised steel specimens were oxidised, they were removed from the furnace and  
26 then cooled to room temperature.  
27  
28  
29  
30  
31  
32  
33  
34

35 All aluminised steel specimens (before and after being oxidized) were characterized by means  
36 scanning electron microscopy (SEM; Jeol JSM 6390) with secondary electron imaging (SEI) for  
37 observing the microstructures and surface morphology of the aluminide layers. Additionally,  
38 Energy-dispersive spectroscopy (EDS) was also performed to analyse their chemical composition  
39 (expressed as atomic percentage, at.%) for determining the phase formed in the aluminide layer.  
40  
41  
42  
43  
44  
45  
46  
47  
48

### <sup>24</sup> 3. Results and discussion

#### 3.1. Characterisation of the aluminide coating

Figure 1a shows the typical microstructure of the aluminised ASTM A26 steel with the coating layer composing to two distinct regions; an aluminium layer (region I) and an intermetallic layer (region II). According to the Fe-Al phase diagram, the aluminide coating that was formed after the steel was dipped into a molten Al (~99 wt.%) bath was dominated by an Al-rich layer and intermetallic compounds composed of  $\text{FeAl}_3$  and  $\text{Fe}_2\text{Al}_5$  phases [14]. EDS results in Figure 1a verified that the chemical compositions of aluminide layer in regions I and II are consistent with Al layer (Fig. 1b; Point A),  $\text{FeAl}_3$  layer (Fig. 1c; Point B), and  $\text{Fe}_2\text{Al}_5$  layer (Fig. 1d; Point C). The aluminide coating consisted of an aluminium layer with low Fe, Si, and Cr concentrations (Fig. 1b). The solubilities of Si in the  $\text{FeAl}_3$  and  $\text{Fe}_2\text{Al}_5$  layers were approximately 1.4 at.% and 2.44 at.%, respectively. EDS results indicate that the solubilities of Cr were lower, 0.19 at.% and 0.33 at.%, respectively (Figs. 1c and 1d). According to the thermodynamic equilibrium, a  $\text{Fe}_2\text{Al}_5$  phase with an orthorhombic structure and a high number of vacancies and defect paths initially formed along the c axis, ultimately contributing to the rapid growth of the  $\text{Fe}_2\text{Al}_5$  phase [15].

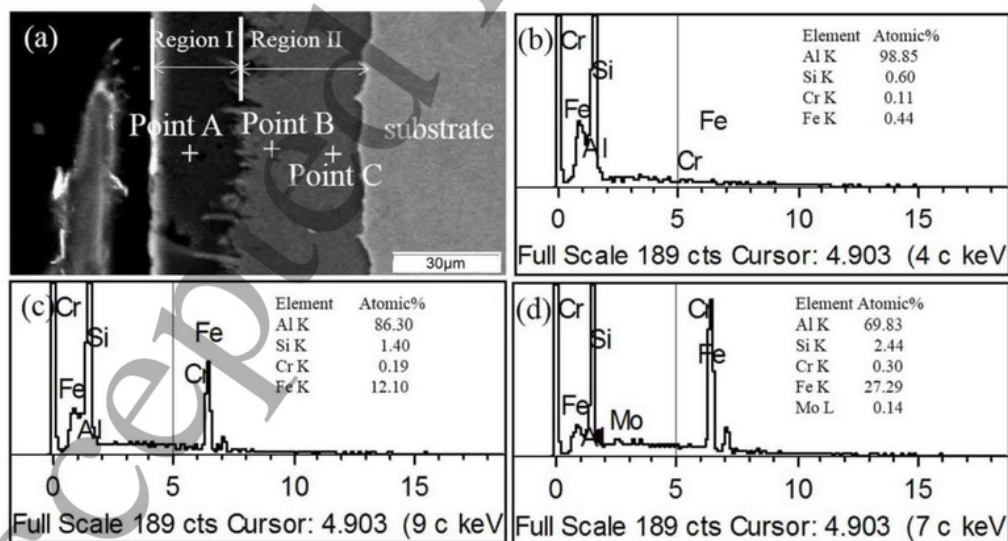
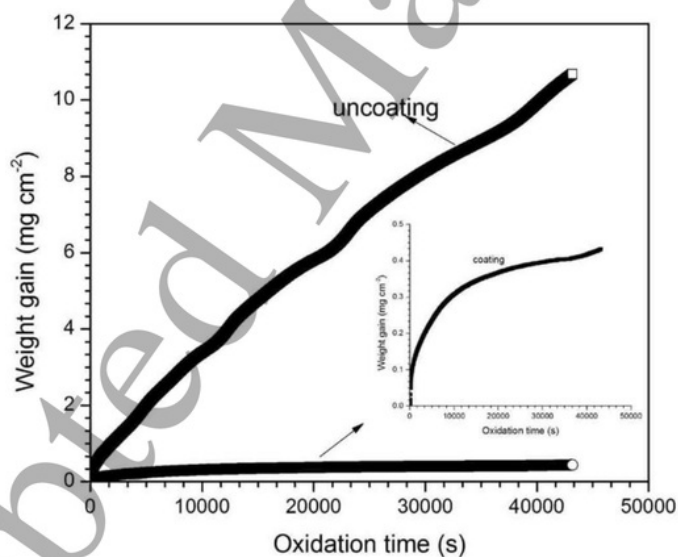


Figure 1. (a) SEI of the cross-sectional morphology of as coated steel and (b-d) EDS spectra of the aluminium and intermetallic layers.

1  
2  
3 The thicknesses of the aluminium and intermetallic layers were approximately 29  $\mu\text{m}$  and 12  
4  $\mu\text{m}$ , respectively. According to Hwang et al. [16], growth of an intermetallic layer and dissolution  
5 of marginal amounts of Fe into the molten aluminium occur simultaneously when steel is in contact  
6 with molten aluminium, and this growth is directly related to the loss of the steel substrate. The  
7 intermetallic layer had a homogeneous, dense structure. No pores and cracks could be observed in  
8 the aluminide coating. The interface between the aluminium topcoat and intermetallic layer was  
9 slightly uneven, and the intermetallic layer/steel substrate interface was relatively smooth because  
10 of its flat structure. This flat structure and the slow growth of the  $\text{Fe}_2\text{Al}_5$  layer are due to the  
11 uniform pearlite microstructure and the high volume fraction of the cementite phase [16],  
12 respectively.  
13  
14  
15  
16  
17  
18  
19  
20  
21  
22  
23  
24  
25  
26



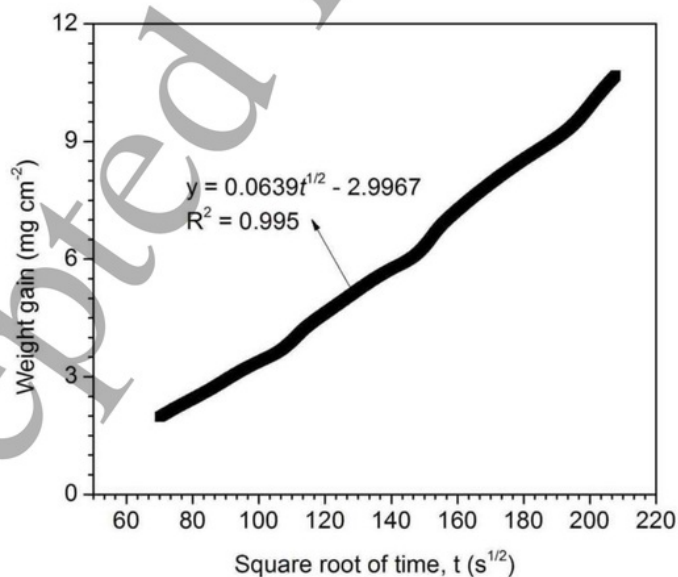
27  
28  
29  
30  
31  
32  
33  
34  
35  
36  
37  
38  
39  
40  
41  
42  
43  
44  
45  
46  
47 Figure 2. Oxidation kinetics curves for the ASTM A29 steel specimens with and without  
48 the aluminium coating.  
49

### 50 51 3.2. Resistance to high-temperature oxidation 52 53 54 55 56 57 58 59 60



1  
2  
3 Figure 2 shows plots of the weight gain of each specimen against the duration of oxidation  
4 indicate that the oxidation of the steel with and without aluminium coatings has parabolic kinetics.  
5  
6 The weight gain of an ASTM A29 steel increased quickly. Hence, a 1.10 wt.% Cr content of the  
7  
8 steel is insufficient for forming a  $\text{Cr}_2\text{O}_3$  layer that protects the steel during oxidation at  $850^\circ\text{C}$  for  
9  
10 12 h.  
11  
12  
13

14 That is, the oxidation kinetics rapidly increased. At the start of oxidation, the kinetics of the  
15 chemical reaction between iron and oxygen ions control the oxidation rate, resulting in rapid  
16 weight gain. Because of the low solubility of Cr in the oxide scale,  $\text{Cr}_2\text{O}_3$  did not form, and  
17 consequently, the oxidation kinetics was rapid (Fig. 2). The  $\text{Cr}_2\text{O}_3$  layer did not grow on the steel  
18 because of the depletion of Cr beneath the iron oxide layer to the lowest concentration [17].  
19 Chromium was depleted toward the interface between the substrate and the iron-rich oxides  $\text{Fe}_3\text{O}_4$   
20 and  $\text{FeO}$ , by conversion to the  $(\text{Fe,Cr})_3\text{O}_4$  phase [4,18].  
21  
22  
23  
24  
25  
26  
27  
28  
29  
30  
31  
32



51  
52  
53  
54 Figure 3. Plot of the weight gain versus the square root of time for an ASTM A29 steel in  
55 air oxidation at  $850^\circ\text{C}$  for 12 h.  
56  
57

As can be observed in Figure 2, the resistance of aluminised steel to high-temperature oxidation markedly increased. The aluminide layer protected the steel substrate against high-temperature oxidation by forming a protective aluminium oxide ( $\text{Al}_2\text{O}_3$ ) layer. At 12 h of oxidation, the weight gain of steel with aluminium coating was approximately  $0.432 \text{ mg cm}^{-2}$ , which is 25-times less than that of the steel without the aluminium coating ( $10.675 \text{ mg cm}^{-2}$ ; Fig. 2).

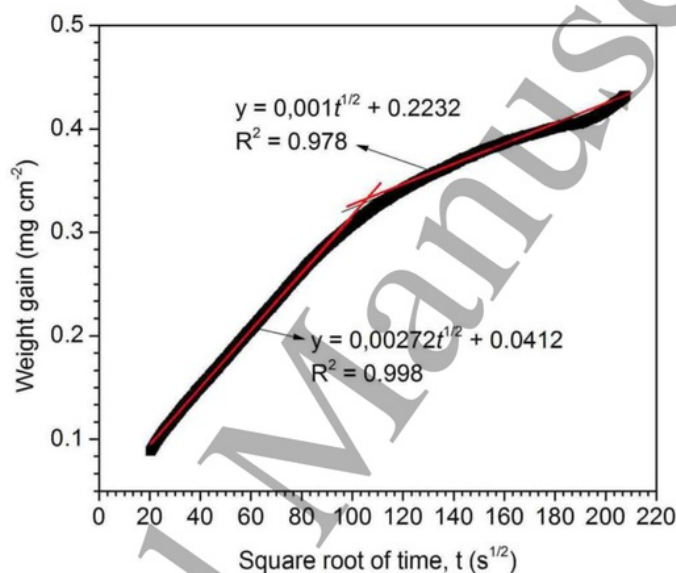


Figure 4. Plots of weight gain versus the square root of time for the aluminised ASTM A29 steel specimens after being oxidised at  $850^\circ\text{C}$  for 12 h.

Plots of the weight gain against exposure time for the uncoated and aluminised steel oxidised at  $850^\circ\text{C}$  (Figs. 3 and 4, respectively) show parabolic behaviour. The parabolic rate constant ( $k_p$ ) for uncoated steel calculated based on the oxidation at 1.4–12 h is approximately  $4,083 \times 10^{-6} \text{ g}^2 \text{ cm}^{-4} \text{ s}^{-1}$ . As shown in Figure 4, the oxidation rate constant ( $k_p = 7.40 \times 10^{-12} \text{ g}^2 \text{ cm}^{-4} \text{ s}^{-1}$ ) was high during the first few hours of oxidation (0.12–2.78 h), subsequently decreasing to a steady-state value ( $k_p = 1.00 \times 10^{-12} \text{ g}^2 \text{ cm}^{-4} \text{ s}^{-1}$ ) at 2.8–12 h. The  $k_p$  values in this study are an order of magnitude similar to those in previously reported studies [7,19].

### 3.3 Characterization of aluminide layers

To elucidate the oxidation behaviour and the formation of intermetallic compounds in the aluminide layer, oxidation tests for aluminised steel specimens were performed. Figure 5a shows a cross-sectional image of the aluminised steel after oxidation for 1 h. The formation mechanism of the intermetallic compound was dominated by interdiffusion of Fe atoms in the substrate and Al atoms in the coating layer during high-temperature exposure. The aluminium and FeAl<sub>3</sub> layers of the as-coated specimen (Fig. 1a) transformed into Fe<sub>2</sub>Al<sub>5</sub> and FeAl<sub>2</sub>. Moreover, the high Si content and low Cr content of the Fe<sub>2</sub>Al<sub>5</sub> layer rapidly decreased in the Fe-rich region because of diffusion coupling between the internal Al atoms and external Fe atoms, which generates regions of FeAl(Cr,Si) particles adjacent to the Fe<sub>2</sub>Al<sub>5</sub> and FeAl<sub>2</sub> layers (Fig. 5a). Also, some voids that formed were dispersed in the outer aluminide layer (Fig. 5a). The intermetallic layer has a thickness of approximately 80 μm and consists of an Al<sub>2</sub>O<sub>3</sub> thin layer on the surface adjacent to a thick Fe<sub>2</sub>Al<sub>5</sub>/FeAl<sub>2</sub> layer and a thin FeAl layer on the steel substrate. The inward diffusion of Al can dominate at this stage, and consumption by oxide growth is probably of minor importance in cavity formation. Also, pores also formed in the aluminide layer (Fig. 5a) because of phase transformation during high-temperature diffusion [20]. In contrast, the outward diffusion of Fe atoms from the steel substrate into the Fe<sub>2</sub>Al<sub>5</sub>/FeAl<sub>2</sub> layer resulted in the instability of the Fe<sub>2</sub>Al<sub>5</sub>/FeAl<sub>2</sub> layer and the formation of FeAl(Cr,Si) particles [7,20] scattered in the Fe<sub>2</sub>Al<sub>5</sub>/FeAl<sub>2</sub> layer (Fig. 5a). EDS spectra (Figs. 5b–d) suggest that Si and Cr dissolved in the Fe<sub>2</sub>Al<sub>5</sub>, FeAl<sub>2</sub>, and FeAl phases and that the Cr and Si content of the FeAl(Cr,Si) phase was substantially greater than that of the FeAl<sub>2</sub> phase (Figs. 5b and 5c). High concentrations of Cr and Si in the FeAl phase are due to the high solubility of both elements in the phase. EDS results for the FeAl<sub>2</sub> phase indicate

that the solubility of Cr in the  $\text{FeAl}_2$  phase is 0.49–1.2 at.% and that the  $\text{Fe}_2\text{Al}_5$  phase has a low Cr concentration (Fig. 1c).

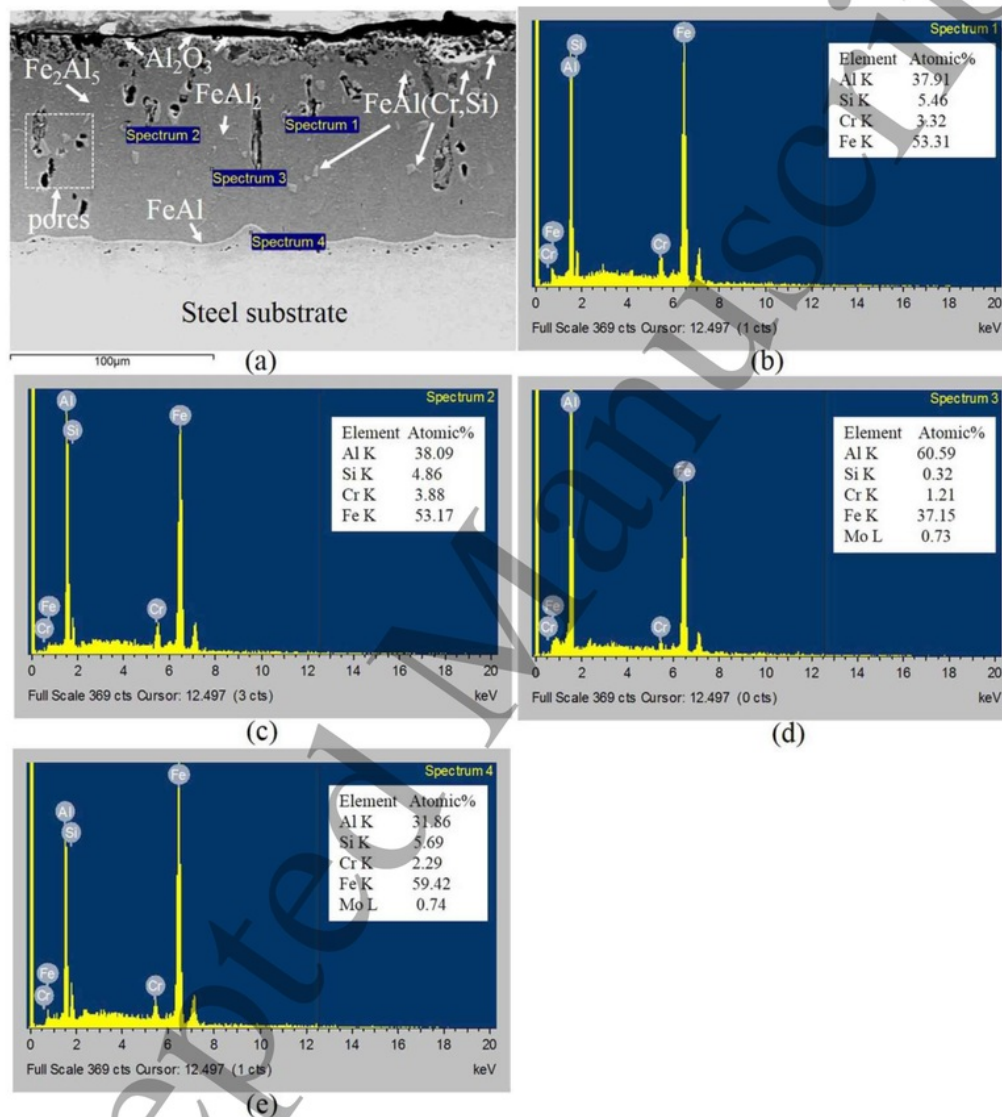


Figure 5. (a) cross-sectional SEM image of the aluminide layer and (b–e) EDS spectra used in element analysis of the aluminide layer formed on the ASTM A29 steel after 1 h oxidation at 850°C.

1  
2  
3 SEM cross-sectional image of the aluminide layer of a specimen oxidised for up to 5 h (Fig. 6a)  
4 suggests that the  $\text{Fe}_2\text{Al}_5$ ,  $\text{FeAl}_2$ , and  $\text{FeAl}$  phases rapidly grew on the steel substrate. Also, a thick  
5  $\text{Al}_2\text{O}_3$  layer formed (Fig. 6b). A continuous  $\text{FeAl}$  layer near the steel substrate gradually thickened  
6 via diffusion of Fe atoms into the  $\text{Fe}_2\text{Al}_5/\text{FeAl}_2$  layer caused by the dilution of aluminium. This  
7 result is consistent with that obtained from the EDS X-ray map analysis (Figs. 6c and 6d). High  
8 Cr and Si concentrations in the  $\text{FeAl}(\text{Cr},\text{Si})$  phases, which became dispersed in the  $\text{Fe}_2\text{Al}_5$  phase  
9 with increasing diffusion time, were still observed in the outer part of the aluminide layer.  
10  
11  
12  
13  
14  
15  
16  
17  
18  
19  
20  
21  
22  
23  
24  
25  
26  
27  
28  
29  
30  
31  
32  
33  
34  
35  
36  
37  
38  
39  
40  
41  
42  
43  
44  
45  
46  
47  
48  
49  
50  
51  
52  
53  
54  
55  
56  
57  
58  
59  
60

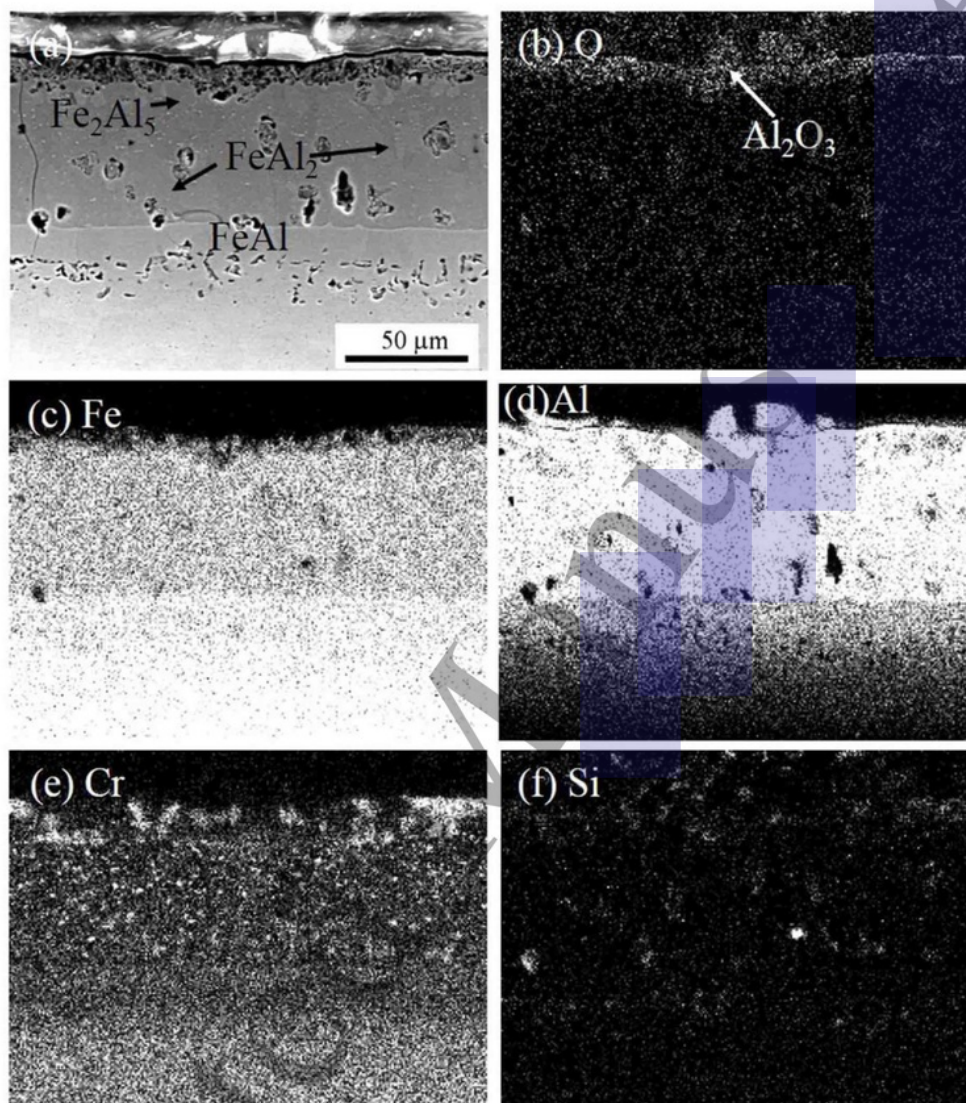


Figure 6. (a) SEM micrograph of the aluminide layer of the aluminised steel oxidised at 850°C for 5 h, and (b–f) the corresponding EDS mapping results for O, Fe, Al, Cr, and Si. This result is consistent with that obtained from X-ray map analysis (Figs. 6e and 6f). The solubilities of Cr and Si in both the FeAl(Cr,Si) particle region (2.29–3.88%) and the continuous FeAl layer (4.86–5.46%) were similar in atomic composition.

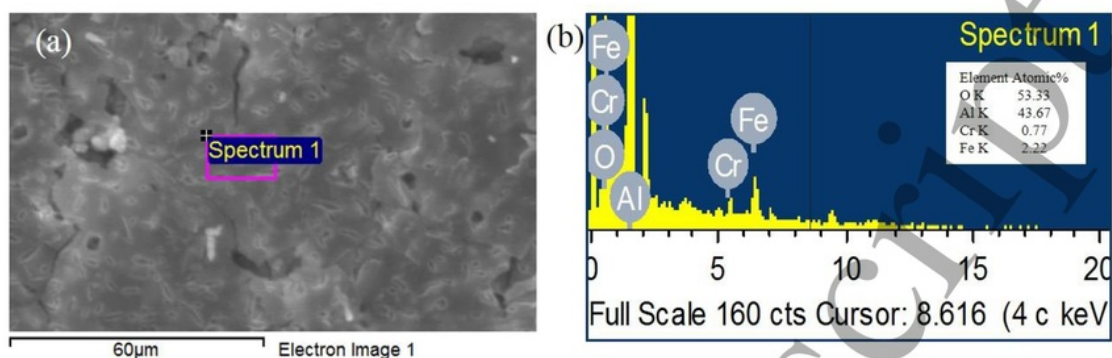


Figure 7. (a) SEM image of the surface morphology of the aluminised steel oxidised at 850°C for 12 h, and (b) results of EDS spectral analysis of O, Al, Cr, and Fe.

The  $k_p$  values of the aluminised steel at the initial stage were greater than those of the aluminised steel during steady-state oxidation (Fig. 4). This was because of the condensation of voids followed by the inward diffusion of oxygen through the voids and cracks, as well as the formation of metastable  $\theta$ - $\text{Al}_2\text{O}_3$  [20] due to the outward diffusion of aluminium. After extended oxidation of aluminised steel (2.8–12 h), the  $k_p$  value of aluminised steel ( $1.00 \times 10^{-12} \text{ g}^2 \text{ cm}^{-4} \text{ s}^{-1}$ ) decreased seven-fold. Figure 7a shows the surface topography of aluminised steel exposed to 12 h of oxidation, as observed by SEI. With increasing oxidation time, the metastable alumina gradually transformed into the  $\alpha$ - $\text{Al}_2\text{O}_3$  phase. Results of EDS element analysis (Fig. 7b) show that Fe and Cr atoms from the aluminide layer penetrated the  $\alpha$ - $\text{Al}_2\text{O}_3$  scale because of the slightly high concentrations of Fe and Cr in the  $\text{Al}_2\text{O}_3$  scale (Fig. 7b). Fe and Cr atoms detected in the alumina scale originated from the  $\text{FeAl}(\text{Cr},\text{Si})$  particles, and Si atoms were undetectable in the alumina scale (Fig. 7b). The Fe and Cr concentrations in the  $\text{Al}_2\text{O}_3$  scale are similar to those reported by Lee et al. [21]. The ability of both Fe and Cr to accelerate the transformation of  $\theta$ - $\text{Al}_2\text{O}_3$  to  $\alpha$ - $\text{Al}_2\text{O}_3$  [22–25] may be the main reason for the decrease in the rate of aluminised-steel oxidation

1  
2  
3 in Figure 4 due to the formation of the  $\alpha$ -Al<sub>2</sub>O<sub>3</sub> scale (Fig. 7b). Thus, a steady-state growth rate  
4  
5 was observed over extended periods.  
6  
7  
8  
9

#### 10 4. Conclusions

11  
12 An ASTM A29 steel was subjected to hot-dip aluminium coating at 700 °C for an immersion  
13  
14 time of 16 s in a molten Al-0.5% Si bath. The total thickness of the aluminide coating on the steel  
15  
16 substrate was 41  $\mu$ m. The Fe<sub>2</sub>Al<sub>5</sub> layer on the steel substrate exhibited a planar structure, high  
17  
18 homogeneity and a strong bond with the steel substrate. Upon coating by hot-dip aluminising  
19  
20 process, the ASTM A29 steel resistance to high-temperature oxidation increased by a factor of 25.  
21  
22 With increasing oxidation time, the oxidation rate constants of the aluminised steel decreased  
23  
24 because of the formation of the protective  $\alpha$ -Al<sub>2</sub>O<sub>3</sub> scale. Growth of this scale was accelerated by  
25  
26 the penetration of Fe and Cr ions into the  $\theta$ -Al<sub>2</sub>O<sub>3</sub> scale, which was predominantly caused by the  
27  
28 high Fe concentration and low Cr concentration (<1%) in the alumina scale.  
29  
30  
31  
32  
33

#### 34 Acknowledgement

35  
36 The authors would like to thank Kemenristekdikti for providing financial support through the  
37  
38 Directorate of Research and Community Service (DRPM) for the National Strategy grant for  
39  
40 financial support with contract No.: 009/SP2H/LT/DRPM/IV/2017.  
41  
42  
43  
44

#### 45 References

- 46  
47 [1] Al-Mazrouee, R.K.S. Raman, High temperature oxidation of Cr–Mo steels in the context  
48  
49 of accelerated rupture testing for creep life prediction, *J. Pressure Vessel Technol.* 129(3)  
50  
51 006) 454–459.  
52  
53 [2] R. Kumar, V.K. Tewari, S. Prakash, Cyclic oxidation behaviour of 1Cr–0.5Mo (T11) boiler  
54  
55 steel and its weldments in air at 900 °C, *Oxid. Met.* 86(1–2) (2016) 89–98.  
56  
57 [3] M.A. Abro, D.B. Lee, Microstructural changes of Al hot-dipped P91 steel during high-  
58  
59 temperature oxidation, *Coatings* 7(2) (2017) 31.  
60



- 1  
2  
3  
4 [4] J. Ehlers, D.J. Young, E.J. Smaardijk, A.K. Tyagi, H.J. Penkalla, L. Singheiser, W.J.  
5 Quadackers, Enhanced oxidation of the 9%Cr steel P91 in water vapour containing  
6 environments, *Corros. Sci.* 48(11) (2006) 3428–3454.  
7 [5] C.J. Wang, S.M. Chen, The high-temperature oxidation behavior of hot-dipping Al–Si coating  
8 on low carbon steel, *Surf. Coat. Technol.* 200 (2006) 6601–6605.  
9 [6] C.J. Wang, M. Badaruddin, The dependence of high temperature resistance of aluminized  
10 steel exposed to water-vapour oxidation, *Surf. Coat. Technol.* 205 (2010) 1200–1205.  
11 [7] Y.Y. Chang, C.C. Tsaur, J.C. Rock, Microstructure studies of an aluminide coating on  
12 9Cr–1Mo steel during high temperature oxidation, *Surf. Coat. Technol.* 200 (22–23) (2006)  
13 6588–6593.  
14 [8] C. Yin, M.X. Zhao, Y.X. Liu, W. Han, Z. Li, Effect of Si on growth kinetics of intermetallic  
15 compounds during reaction between solid iron and molten aluminum, *Trans. Nonferrous Met.*  
16 *Proc. China* 23 (2013) 556–561.  
17 [9] A.S. Sree, E.R. Kumar, Effect of heat treatment and silicon concentration on microstructure  
18 and formation of intermetallic phases on hot dip aluminized coating on Indian RAFMS,  
19 *Corros. Sci. Technol.* 65(2) (2014) 282–291.  
20 [10] K. Zaba, Selected problems of formability of aluminised steel plates, *Arch. Civ. Mech. Eng.*  
21 12(2) (2012) 163–170.  
22 [11] M. Badaruddin, R.T. Riza, Zulhanif, The effect of diffusion treatment on the mechanical  
23 properties of hot-dip aluminum coating on AISI P20 steel, *AIP Conf. Proc.* 1983 (2018)  
24 50004.  
25 [12] W.J. Cheng, C.J. Wang, High-temperature oxidation behavior of hot-dipped aluminide mild  
26 steel with various silicon contents, *Appl. Surf. Sci.* 274 (2013) 258–265.  
27 [13] M. Badaruddin, C.J. Wang, Y. Saputra, A.K. Rivai, High temperature corrosion of aluminized  
28 AISI 4130 steel with the different composition of NaCl/Na<sub>2</sub>SO<sub>4</sub> deposits, *Makara J. Technol.*  
29 19(2) (2015) 45–50.  
30 [14] U.R. Kattner, B.P. Burton, Alloy Phase Diagrams, Vol. 3, ASM International, USA, 1992.  
31 [15] W.J. Cheng, C.J. Wang, Growth of intermetallic layer in the aluminide mild steel during hot-  
32 dipping, *Surf. Coat. Technol.* 204(6–7) (2009) 824–828.  
33 [16] S.H. Hwang, J.H. Song, Y.S. Kim, Effects of carbon content of carbon steel on its dissolution  
34 into a molten aluminum alloy, *Mater. Sci. Eng. A* 390(1–2) (2005) 437–443.  
35 [17] R.K.S. Raman, Relevance of High-Temperature Oxidation in Life Assessment and  
36 Microstructural Degradation of Cr-Mo Steel Weldments, *Metall. Mat. Trans. A* 30 (12) (2000)  
37 3101–3108.  
38 [18] D. Chaliampalias, G. Vourlias, E. Pavlidou, K. Chrissafis, High temperature oxidation of Cr–  
39 Mo–V tool steel in carbon dioxide, *J. Therm. Anal. Calorim.* 113 (3) (2013) 1309–1315.  
40 [19] Y.Y. Chang, W.J. Cheng, C.J. Wang, Growth and surface morphology of hot-dip Al–Si on  
41 9Cr–1Mo steel, *Mater. Charac.* 60(2) (2009) 144–149.  
42 [20] J. Cheng, C.J. Wang, Effect of chromium on the formation of intermetallic phases in  
43 hot-dipped aluminide Cr–Mo steels, *Appl. Surf. Sci.* 277 (2013) 139–145.  
44 [21] D.B. Lee, G.Y. Kim, J.G. Kim, The oxidation of Fe<sub>3</sub>Al–(0, 2, 4, 6%)Cr alloys at 1000 °C,  
45 *Mater. Sci. Eng. A* 339(1–2) (2003) 109–119.  
46 [22] S. Hayashi, Y. Takada, S. Yoneda, S. Ukai, Metastable-Stable Phase Transformation  
47 Behavior of Al<sub>2</sub>O<sub>3</sub> Scale Formed on Fe–Ni–Al Alloys, *Oxid. Met.* 86(1) (2016) 151–164.  
48  
49  
50  
51  
52  
53  
54  
55  
56  
57  
58  
59  
60

- 1  
2  
3 [23] Q. Zhan, W. Zhao, H. Yang, Y. Hatano, X. Yuan, T. Nozaki, X. Zhu, Formation of  $\alpha$ -alumina  
4 scales in the Fe–Al(Cr) diffusion coating on China low activation martensitic steel, *J. Nucl.*  
5 *Maters.* 464 (2015) 135–139.  
6  
7 [24] Y. Huang, X. Peng, The promoted formation of  $\alpha$ -Al<sub>2</sub>O<sub>3</sub> scale on a nickel aluminide with  
8 surface Cr<sub>2</sub>O<sub>3</sub> particles, *Corros. Sci.* 112 (2016) 226–232.  
9  
10 [25] A. Shaaban, S. Hayashi, K. Azumi, Promotion of  $\alpha$ -Al<sub>2</sub>O<sub>3</sub> formation on an Ni–Al alloy using  
11 a Ni–Fe<sub>2</sub>O<sub>3</sub> nano-composite seeding layer, *Surf. Coat. Technol.* 266 (2015) 113–121.  
12  
13  
14  
15  
16  
17  
18  
19  
20  
21  
22  
23  
24  
25  
26  
27  
28  
29  
30  
31  
32  
33  
34  
35  
36  
37  
38  
39  
40  
41  
42  
43  
44  
45  
46  
47  
48  
49  
50  
51  
52  
53  
54  
55  
56  
57  
58  
59  
60

# The resistance of an aluminide coating on a high-strength ASTM A29 steel subjected to a temperature of 850

## ORIGINALITY REPORT

**26%**

SIMILARITY INDEX

**16%**

INTERNET SOURCES

**23%**

PUBLICATIONS

**14%**

STUDENT PAPERS

## PRIMARY SOURCES

**1**

[eprints.gla.ac.uk](http://eprints.gla.ac.uk)

Internet Source

**7%**

**2**

Submitted to B.S.Abdur Rahman Crescent  
Institute of Science & Technology

Student Paper

**3%**

**3**

[media.neliti.com](http://media.neliti.com)

Internet Source

**2%**

**4**

Chaur Jeng Wang, Mohd. Badaruddin. "The  
dependence of high temperature resistance of  
aluminized steel exposed to water-vapour  
oxidation", Surface and Coatings Technology,  
2010

Publication

**1%**

**5**

[repository.lppm.unila.ac.id](http://repository.lppm.unila.ac.id)

Internet Source

**1%**

**6**

Badaruddin, Mohammad, Harnowo Supriadi,  
and Erwin. "Improvement of the High  
Temperature Oxidation of 1.10Cr-0.25Mo Steel  
at 850°C by Hot-dip Al Coating", Procedia

**1%**

## Engineering, 2012.

Publication

- 
- |    |  |     |
|----|--|-----|
| 7  | Vaibhav Bhavsar, Tarandip Singh Dang, Hiren Patel, Bharati Rehani, N.I. Jamnapara.<br>"Structural characterization of aluminized steel heat treated in different environments", Surface and Coatings Technology, 2018<br>Publication | 1%  |
| 8  | <a href="http://www.scientific.net">www.scientific.net</a><br>Internet Source  | 1%  |
| 9  | <a href="http://ceramics.onlinelibrary.wiley.com">ceramics.onlinelibrary.wiley.com</a><br>Internet Source  | 1%  |
| 10 | Submitted to University of Birmingham<br>Student Paper   | 1%  |
| 11 | Cheng, Wei-Jen, and Chaur-Jeng Wang. "High-temperature oxidation behavior of hot-dipped aluminide mild steel with various silicon contents", Applied Surface Science, 2013.<br>Publication   | 1%  |
| 12 | M. Badaruddin, R. Tommy Riza, Zulhanif. "The effect of diffusion treatment on the mechanical properties of hot-dip aluminum coating on AISI P20 steel", AIP Publishing, 2018<br>Publication  | 1%  |
| 13 | <a href="http://repo-nkm.batan.go.id">repo-nkm.batan.go.id</a><br>Internet Source  | <1% |
-

14

Naoki Takata, Manamu Nishimoto, Satoru Kobayashi, Masao Takeyama. "Crystallography of Fe 2 Al 5 phase at the interface between solid Fe and liquid Al", Intermetallics, 2015

Publication

&lt;1%

15

[www.mdpi.com](http://www.mdpi.com)

Internet Source

&lt;1%

16

Submitted to Higher Education Commission Pakistan

Student Paper

&lt;1%

17

[www.science.gov](http://www.science.gov)

Internet Source

&lt;1%

18

Mohammadi, T., and X. Huang. "Effect of Al and Ti addition on performance of stainless steel 310 in supercritical water", Corrosion Engineering Science and Technology, 2015.

Publication

&lt;1%

19

B. Lemmens, H. Springer, M. Peeters, I. De Graeve, J. De Strycker, D. Raabe, K. Verbeken. "Deformation induced degradation of hot-dip aluminized steel", Materials Science and Engineering: A, 2018

Publication

&lt;1%

20

A. Al-Mazrouee, R. K. Singh Raman. "High Temperature Oxidation of Cr-Mo Steels in the Context of Accelerated Rupture Testing for

&lt;1%

Creep Life Prediction", Journal of Pressure Vessel Technology, 2007

Publication

---

21 Wang, C.J.. "The dependence of high temperature resistance of aluminized steel exposed to water-vapour oxidation", Surface & Coatings Technology, 20101125

Publication

---

22 Xiang, Xin, Xiaolin Wang, Guikai Zhang, Tao Tang, and Xinchun Lai. "Preparation technique and alloying effect of aluminide coatings as tritium permeation barriers: A review", International Journal of Hydrogen Energy, 2015.

Publication

---

23 Submitted to National Institute Of Technology, Tiruchirappalli

Student Paper

---

24 Cheng, W.J.. "Characterization of intermetallic layer formation in aluminide/nickel duplex coating on mild steel", Materials Characterization, 201207

Publication

---

25 D. Deduytsche, C. Detavernier, R. L. Van Meirhaeghe, J. L. Jordan-Sweet, C. Lavoie. "Formation and morphological stability of NiSi in the presence of W, Ti, and Ta alloying elements", Journal of Applied Physics, 2007

26 Mohammad Badaruddin, Chaur Jeng Wang, Yudhistyra Saputra, Abu Khalid Rivai. "High Temperature Corrosion of Aluminized AISI 4130 Steel with the Different Composition of NaCl/Na<sub>2</sub>SO<sub>4</sub> Deposits", Makara Journal of Technology, 2015

Publication

---

27 Submitted to Universitas Negeri Jakarta

Student Paper

---

28 Submitted to International Islamic University Malaysia

Student Paper

---

29 [mdpi.com](http://mdpi.com)

Internet Source

---

30 Wei-Jen Cheng, Yi-Jhang Liao, Chaur-Jeng Wang. "Effect of nickel pre-plating on high-temperature oxidation behavior of hot-dipped aluminide mild steel", Materials Characterization, 2013

Publication

---

31 Lee, D.. "The oxidation of Fe<sup>3</sup>Al-(0, 2, 4, 6%)Cr alloys at 1000<sup>o</sup>C", Materials Science & Engineering A, 20030102

Publication

---

32 [uad.portalgaruda.org](http://uad.portalgaruda.org)

Internet Source

<1%

33

Cheng, W.J.. "Microstructural evolution of intermetallic layer in hot-dipped aluminide mild steel with silicon addition", Surface & Coatings Technology, 20110625

Publication

<1%

Exclude quotes Off

Exclude matches Off

Exclude bibliography Off



# The resistance of an aluminide coating on a high-strength ASTM A29 steel subjected to a temperature of 850

---

GRADEMARK REPORT

---

FINAL GRADE

**/0**

GENERAL COMMENTS

**Instructor**

---

PAGE 1

---

PAGE 2

---

PAGE 3

---

PAGE 4

---

PAGE 5

---

PAGE 6

---

PAGE 7

---

PAGE 8

---

PAGE 9

---

PAGE 10

---

PAGE 11

---

PAGE 12

---

PAGE 13

---

PAGE 14

---

PAGE 15

---

PAGE 16

---

PAGE 17

---